EBERHART, M. E., DONOVAN, M. M. & OUTLAW, R. A. (1992). *Phys. Rev. B*, **46**, 12744–12747.
GATTI, C., FANTUCCI, P. & PACCHIONI, G. (1987). *Theor. Chim. Acta*, **72**, 433–458.
GÖTTLICHER, S. & WÖLFEL, E. (1959). *Z. Electrochem.* **63**, 891–901.
HAHN, T. (1983). *International Tables for Crystallography*, Vol. A. Boston: Reidel. (Present distributor Kluwer Academic Publishers, Dordrecht.)
JEFFREY, G. A. & PINIELLA, J. F. (1991). Editors. *The Application of Charge-Density Research to Chemistry and Drug Design. NATO Adv. Study Inst. Ser. B*, No. 250.
JOHNSON, C. K. (1977). Am. Crystallogr. Assoc. Winter Meet., Asilomar. Abstracts, p. 30.
KAPPKHAN, M., TSIRELSON, V. G. & OZEROV, R. P. (1989). *Dokl. Phys. Chem.* **303**, 1025–1029.
KITTEL, C. (1986). *Introduction to Solid State Physics*. New York: Wiley.
LAU, C. D. H., BADER, R. F. W., HERMANSSON, K. & BERKOVITCH-YELLIN, Z. (1986). *Chem. Scr. Abstr.* **26**, 476.
LOBANOV, N. N., TSIRELSON, V. G. & BELOKONAVA, E. L. (1988). *Russ. J. Inorg. Chem.* **33**, 1740–1744.
LU, Z. W. & ZUNGER, A. (1992). *Acta Cryst.* A**48**, 545–554.
MEI, C., EDGECOMBE, K. E., SMITH, V. H. & HEILINGBRUNNER, A. (1993). *Int. J. Quantum Chem.* **48**, 287–293.
ORLANDO, R., DOVESI, R., ROETTI, C. & SAUNDERS, V. R. (1990). *J. Phys. Condens. Matter*, **2**, 7769–7789.
PISANI, C., DOVESI, R. & ORLANDO, R. (1992). *Int. J. Quantum Chem.* **42**, 5–33.
PISANI, C., DOVESI, R. & ROETTI, C. (1988). *Hartree–Fock Ab Initio Treatment of Crystalline Systems, Lecture Notes in Chemistry*, Vol. 48. Heidelberg: Springer-Verlag.
POPELIER, P. L. A. & BADER, R. F. W. (1994). *J. Phys. Chem.* **98**, 4473–4481.
RUNTZ, G. R., BADER, R. F. W. & MESSER, R. (1977). *Can. J. Chem.* **55**, 3040–3045.
SAKA, T. & KATO, N. (1986). *Acta Cryst.* A**42**, 469–478.
SAKATA, M. & SATO, M. (1990). *Acta Cryst.* A**46**, 263–270.
SCHWINGER, J. (1951). *Phys. Rev.* **82**, 914–927.
SLATER, J. C. (1934). *Phys. Rev.* **45**, 794–801.
SLATER, J. C. (1965). *Quantum Theory of Molecules and Solids*, pp. 14–23. New York: McGraw-Hill.
SMITH, V. H., PRICE, P. F. & ABSAR, I. (1977). *Isr. J. Chem.* **16**, 187–197.
SPACKMAN, M. A. (1986). *Acta Cryst.* A**42**, 271–281.
WENTZKOVITCH, R. M., CHANG, K. J. & COHEN, M. L. (1986). *Phys. Rev. B*, **34**, 1071–1079.
WEYRICH, K. H., BREY, L. & CHRISTENSEN, N. E. (1988). *Phys. Rev. B*, **38**, 1392–1396.
WIGNER, E. & SEITZ, F. (1933). *Phys. Rev.* **43**, 804–810.
ZHANG, S. B. & COHEN, M. L. (1987). *Phys. Rev. B* **35**, 7604–7610.
ZOU, P. F. (1993). PhD thesis, McMaster Univ., Hamilton, Ontario, Canada.

Acta Cryst. (1994). A**50**, 725–730

Study of Thermal Behaviour of Oxygen in Silicon Crystals by Analysis of X-ray *Pendellösung* Fringes

BY MING LI, ZHEN-HONG MAI AND SHU-FAN CUI

Institute of Physics, Chinese Academy of Sciences, PO Box 603, *Beijing* 100080, *People's Republic of China*

(*Received* 12 *October* 1993; *accepted* 21 *April* 1994)

Abstract

The thermal behaviour of oxygen in Czochralski (CZ) silicon and magnetic Czochralski (MCZ) silicon crystals was investigated by analysis of *Pendellösung* fringes based on the statistical theory of X-ray dynamical diffraction. The size and the density of oxygen precipitates were determined for different annealing temperatures and/or different times. It was observed that oxide precipitates in the samples increase in size and decrease in density with time during isothermal annealing at 1023 K. The precipitation in MCZ silicon approaches saturation level after annealing for 250 h. It was found that the size of precipitates increases rapidly with annealing temperature in isochronal annealing for 18 h. Comparison of the results of MCZ silicons with those of CZ silicons shows that MCZ crystals are thermally more stable. This suggests that magnetic fields can control the oxygen concentration effectively and that the MCZ and CZ silicon have different thermal behaviours. A powerful technique for detecting microdefects of nanometre size and random distribution is described.

1. Introduction

Silicon crystals grown by the Czochralski (CZ) method or by the Czochralski method in a magnetic field (MCZ) contain supersaturated O atoms that come from the silica crucible. This high concentration of O atoms remains in metastable solid solution during the cooling of as-grown silicon ingots. Although there is a considerable amount of literature concerning the thermal behaviour of oxygen precipitates, the mechanism of their formation in silicon is still an important problem for ultra large scale integrated-circuit fabrication (Claeys & Vanhellemont, 1993). Since the spatial resolu-

tion of conventional X-ray section-topographic techniques is not good enough to detect randomly distributed microdefects of nanometre size (Patel, 1973), a statistical theory of X-ray dynamical diffraction has recently been developed (Kato, 1980). According to Kato's theory, small and randomly distributed precipitates in crystals, which are impossible to detect by conventional X-ray topography, will affect the period of *Pendellösung* fringes owing to the reduction in reflection strength caused by lattice distortions surrounding the precipitates. This effect is characterized by a static Debye–Waller factor (DWF) (Sugita, Sugiyama, Iida & Kawata, 1987). On the other hand, the size and the density of precipitates can be determined by the change in *Pendellösung* fringes in section topographs.

In this paper, we report some results of the thermal behaviour of oxygen in both CZ and MCZ silicon crystals annealed at different temperatures and/or for different times. The intensity distributions of *Pendellösung* fringes in section topographs of both MCZ and CZ silicons that had undergone systematic heat treatments were measured by a microdensitometer. The average size and the density of precipitates were determined using a curve-fitting method. It is shown that MCZ and CZ silicon exhibit different thermal behaviours.

2. Theoretical background

According to Kato's statistical theory of dynamical diffraction, the intensity distribution profile of *Pendellösung* fringes in Laue geometry is given by (Sugita, Sugiyama, Iida & Kawata, 1987; Iida, Sugiyama, Sugita & Kawata, 1988)

$$I_h = C_1|\beta E|^2 \exp(-\mu t/\cos\theta_B)[|J_0(\beta E\xi)|^2 + |\cos 2\theta_B|^2 \times |J_0(|\cos 2\theta_B|\beta E\xi)|^2] + C_2 + C_3 x/w, \quad (1)$$

where J_0 is the zeroth-order Bessel function and its arguments β, ξ and E (static DWF) are given by

$$\beta = (2r_e\lambda F_h)/v_0 \sin 2\theta_B, \quad (2)$$

$$E = \exp(-L_h), \quad (3)$$

$$\xi = t\{(1/\tan\alpha) - [1/\tan(\alpha + 2\theta_B)]\} \times [\sin\alpha \sin(\alpha + 2\beta_B)]^{1/2}\{[x(w-x)]^{1/2}/w\}, \quad (4)$$

where μ is the linear absorption coefficient, θ_B the Bragg angle, λ the wavelength, v_0 the unit-cell volume, r_e the classical electron radius, F_h the hth-order structure factor including the temperature factor, t the thickness of the sample and α the angle between the incident beam and the sample surface. C_1, C_2 and C_3 are three adjustable parameters. C_1 and C_2 stand for the amplitudes of the oscillatory dynamical term and the nonoscillating kinematical term, respectively, and C_3 represents the gradient in the background intensity on the photographic plate. The geometrical parameters w and x, which specify the position on the section topograph, are shown in Fig. 1.

By a curve-fitting method, the static Debye–Waller factors E can be determined and from these the average size and the density of oxygen precipitates can be estimated. According to solid-state physics (Dederichs, 1973), when the concentration of precipitates c_0 and the lattice displacement field $\mathbf{u}(\mathbf{r})$ around the precipitates are small, the parameter L_h in (3) can be expressed by a continuum approximation

$$L_h = (c/v_0)\int\{1 - \cos[\mathbf{h}\cdot\mathbf{u}(\mathbf{r})]\}\mathrm{d}\mathbf{r}, \quad (5)$$

where c is given by the ratio of the number of precipitates to the number of host atoms. With the assumption that the morphology of the precipitates is spherical, the displacement $\mathbf{u}(\mathbf{r})$ around the precipitates is given by

$$\mathbf{u}(\mathbf{r}) = \begin{cases} \varepsilon\mathbf{r} & r < R_0 \\ (\varepsilon R_0^3/r^3)\mathbf{r} & r > R_0 \end{cases}, \quad (6)$$

where R_0 is the radius of precipitates and ε is the strain. Substituting (6) into (5), we obtain

$$L_h(A) = (cV/v_0)\left(1 + 3[(A\cos A/A^3) - (\sin A/A^3)] + 3\int_1^\infty \{1 - [\sin(A/x^2)/(A/x^2)]\}x^2\mathrm{d}x\right), \quad (7)$$

where $A = h\varepsilon R_0$, $x = r/R_0$ and $V = 4\pi R_0^3/3$ is the volume of precipitates.

Comparing the calculated L_h with the experimental L_h, we obtain the R_0 and the c_0 of precipitates.

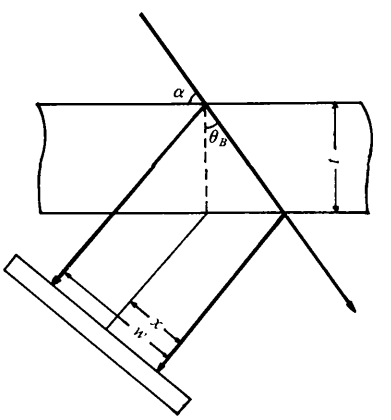

Fig. 1. Geometrical parameters of section topography.

Here, we assume for the sake of simplicity that SiO_2 precipitates have a spherical shape during the precipitation process. The proportional constant in (7), cV/v_0, is given by

$$cV/v_0 = [v(SiO_2)/2]n, \tag{8}$$

where $v(SiO_2)$ is the volume of one molecule of SiO_2 precipitate and n is the total amount of precipitated oxygen that is evaluated by the infrared absorption measurement at wave number 1107 cm^{-1}.

3. Experimental

The specimens studied here were n-type (111) and/or (001) silicon wafers. They were cut from dislocation-free silicon ingots grown by CZ and/or MCZ methods. The oxygen contents are 1×10^{18} cm^{-3} for CZ silicon and 5×10^{17} cm^{-3} for MCZ silicon and the resistances are $< 10\ \Omega$ for CZ silicon and $\sim 10\ \Omega$ for MCZ silicon. Both sides of the wafers were polished by a standard chemical–mechanical method. Two kinds of heat treatment, isothermal and iso-

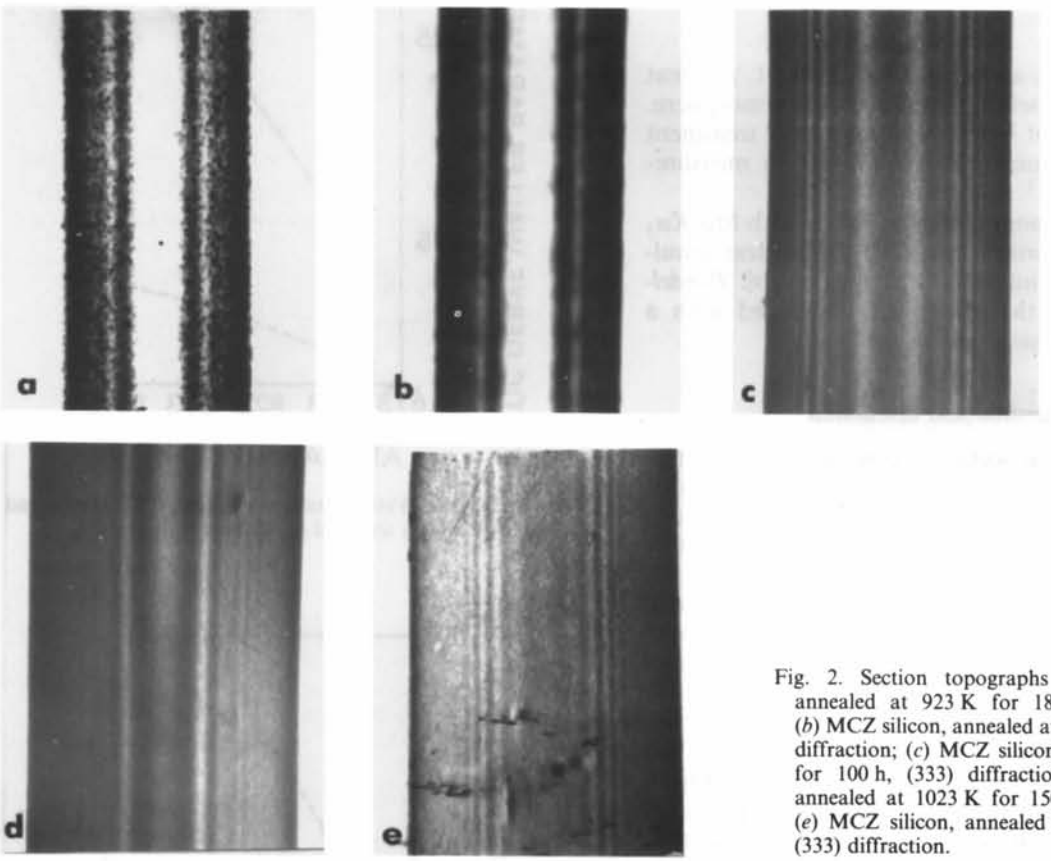

Fig. 2. Section topographs of (*a*) CZ silicon, annealed at 923 K for 18 h, (440) diffraction; (*b*) MCZ silicon, annealed at 923 K for 18 h, (440) diffraction; (*c*) MCZ silicon, annealed at 1023 K for 100 h, (333) diffraction; (*d*) MCZ silicon, annealed at 1023 K for 150 h, (333) diffraction; (*e*) MCZ silicon, annealed at 1023 K for 250 h, (333) diffraction.

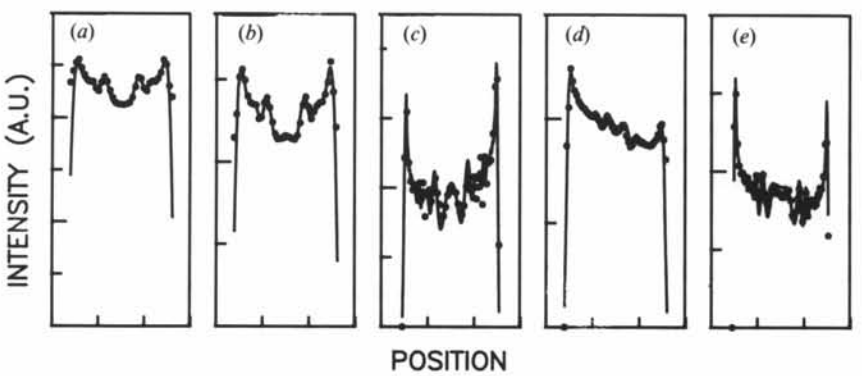

Fig. 3. Intensity distributions of the section topographs corresponding to those in Fig. 2. The solid lines are theoretical curves.

Table 1. *Specimen parameters*

The precipitated oxygen was measured after heat treatment.

Specimen	Growth method	Temperature (K)	Time (h)	Precipitated oxygen (10^7 atoms cm^{-3})
1	MCZ	723	18	0.11
2	MCZ	923	18	0.35
3	MCZ	1073	18	0.37
4	CZ	723	18	1.90
5	CZ	923	18	3.40
6	CZ	1073	18	3.20
7	MCZ	1023	50	1.34
8	MCZ	1023	100	1.39
9	MCZ	1023	150	1.47
10	MCZ	1023	250	1.52
11	MCZ	1023	400	1.70

chronal, were used, as shown in an Table 1. All heat treatments were carried out in an N_2 atmosphere. The oxygen content before and after heat treatment was determined from infrared absorption measurements at 1107 cm^{-1}.

X-ray section topographs were taken with Mo $K\alpha_1$ radiation and recorded on Ilford *L*4 nuclear emulsion plates. The intensity distribution of *Pendellösung* fringes on the plates was measured with a standard microdensitometer.

4. Results and discussion

Fig. 2 shows typical section topographs of specimen nos. 5, 2, 8, 9 and 10 and the *Pendellösung* fringes are clearly evident. However, individual precipitates cannot be seen in the section topographs except in Fig. 2(*e*). However, the change in the period of *Pendellösung* fringes caused by small precipitates can be easily revealed. Figs. 3(*a*) to (*e*) show comparisons between experimental and theoretical intensity distributions corresponding to Figs. 2(*a*) to (*e*), respectively. The solid lines are theoretical curves best fitted to the experimental points by using the optimum parameters C_1, C_2, C_3 and E in (1). Fig. 4 shows the static DWF L of isochronal samples as a function of annealing temperature. It is evident that as the temperature increases the value of L increases. Moreover, the value of L for MCZ silicon is much smaller than that for CZ silicon, especially at higher temperature. This means that the MCZ silicon has a higher thermal stability.

Fig. 5 shows the static DWF L of isothermal samples as a function of annealing time. It can be seen that with the increase of annealing time the value of L increases until $t \geq 250$ h, where L becomes a maximum. The precipitates approach saturation after 250 h of annealing.

The dependences of R_0 and c_0 on the annealing time at 1023 K, obtained from the static DWF and the measured concentration of precipitated oxygen, are shown in Figs. 6 and 7, respectively. These dependences can be explained as follows (Gösele & Tan, 1982). In the initial stage of annealing, the precipitates nucleate with small size and high density, but only those whose actual sizes are larger than the critical value will grow throughout the whole thermal treatment, while those with sizes smaller than the

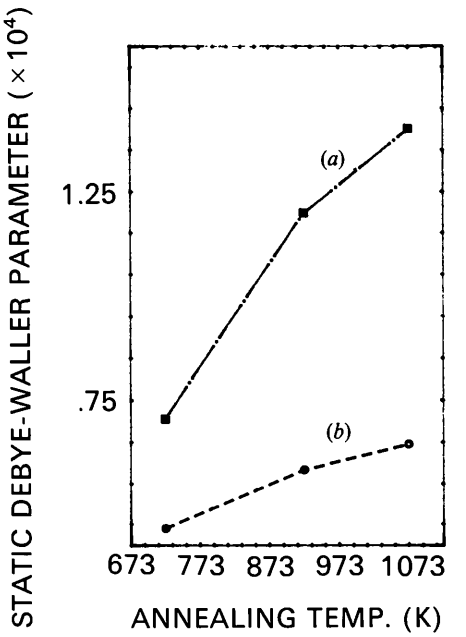

Fig. 4. Static Debye–Waller parameters L for (*a*) CZ silicon and (*b*) MCZ silicon annealed at different temperatures.

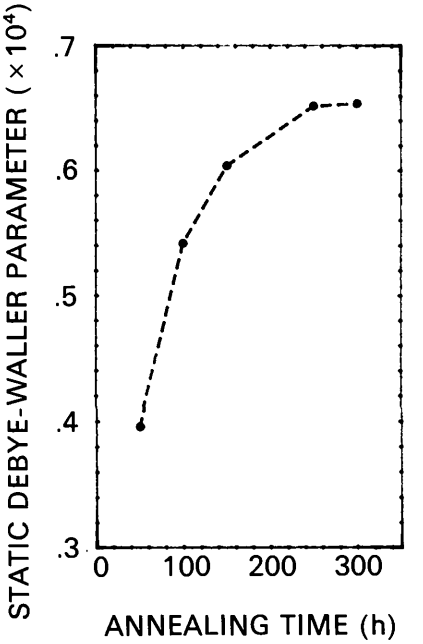

Fig. 5. Static Debye–Waller parameters L for MCZ silicon annealed at 1023 K for different times.

critical value will dissolve. This leads to increase of R_0 and decrease of c_0 with increase in annealing time. After annealing for a long time, say 250 h in Figs. 6 and 7, the precipitation tends to a saturation state.

In the isochronal annealing for 18 h, a rapid increase of R_0 with increasing annealing temperature is observed in Fig. 8. This means that both the diffusivity of interstitial oxygen and the critical radius of the precipitates are larger at higher temperature.

By comparing the results of MCZ silicon with those of CZ silicon in Fig. 8 and 9, one can see that both the average size and the density of the precipitates in MCZ silicon are much smaller than those in CZ silicon. Moreover, the increased rate of increase of R with temperature for MCZ silicon is

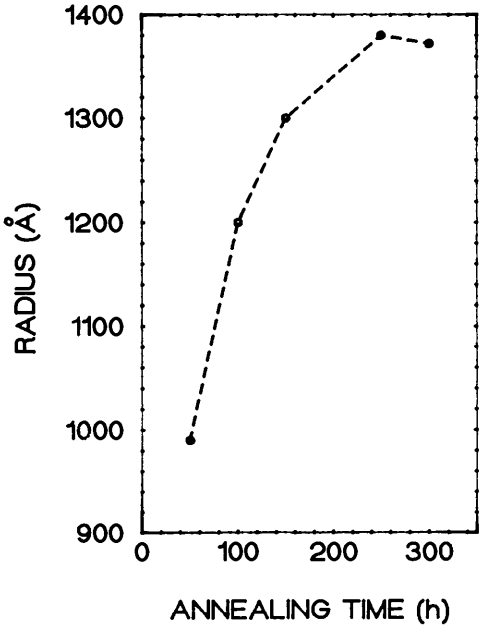

Fig. 6. The radius R_0 of the precipitates in MCZ silicon as a function of the annealing time.

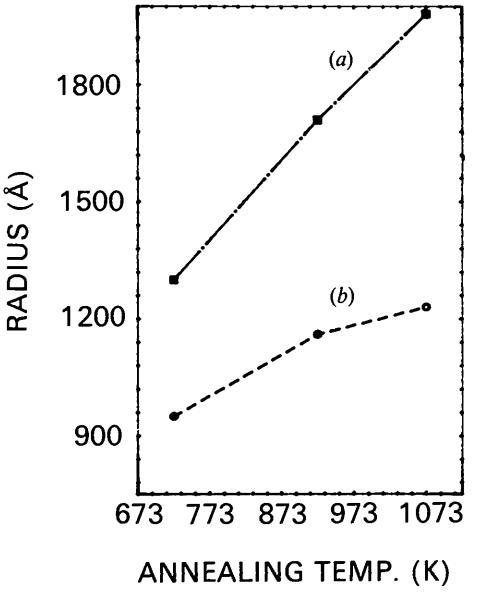

Fig. 8. The radius R_0 of the precipitates as a function of the annealing temperature for (*a*) CZ silicon and (*b*) MCZ silicon.

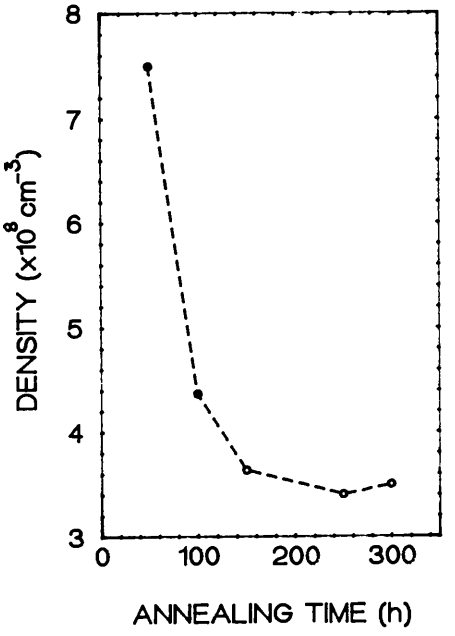

Fig. 7. The density c_0 of the precipitates in MCZ silicon as a function of the annealing time.

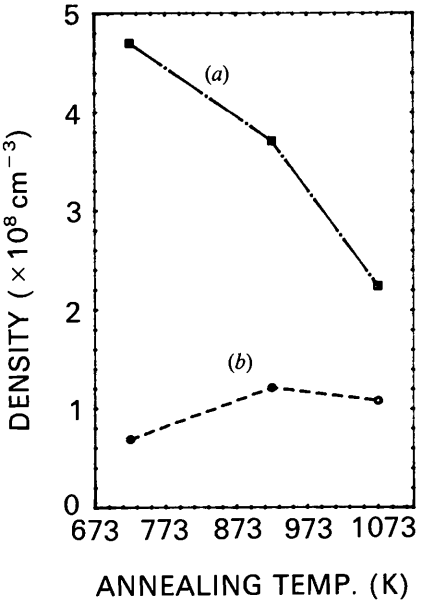

Fig. 9. The density c_0 of the precipitates as a function of the annealing temperature for (*a*) CZ silicon and (*b*) MCZ silicon.

slower than that for CZ silicon. This is explicable by the fact that the concentration of interstitial oxygen in as-grown MCZ silicons is smaller than that in as-grown CZ silicons. For isochronal annealing, the precipitate density in MCZ silicon increases at first with temperature then decreases above 923 K, while the tendency towards small density with CZ silicon occurs at a relatively lower temperature, since precipitates with larger size than the critical radius grow up more rapidly in CZ silicon than those in MCZ silicon under the same thermal conditions. Mai *et al.* (1990) have reported that thermal donor generation in MCZ silicon is much lower than in CZ silicon. All these factors confirm the above arguments, *i.e.* MCZ silicon is more thermally stable than CZ silicon. Furthermore, this confirms the observation that magnetic fields can effectively control the oxygen concentration. Since the oxygen concentration in MCZ silicon is smaller than that in CZ silicon, they have different thermal behaviours.

5. Concluding remarks

We have investigated the thermal behaviour of oxygen in silicon by analysing the *Pendellösung* fringes in X-ray section topographs. For isothermal annealing at 1023 K, the average size of precipitates increases with the annealing time while the precipitate density decreases. The precipitation approaches a saturation level after 250 h annealing for MCZ silicon. For isochronal annealing for 18 h, the size of precipitates increases rapidly with increasing temperature. This results from both the diffusivity of the interstitial oxygen and the critical radius of precipitates being larger at higher temperature. Comparison of the results for MCZ silicon with those for CZ silicon shows that MCZ silicon crystals are more thermally stable than CZ silicons. The thermal donor generation is also weaker in MCZ silicons than in CZ silicons. This suggests that magnetic fields can control the oxygen concentration effectively and can provide high-quality silicon crystals. Moreover, the MCZ and the CZ silicons have different thermal behaviours. The method described here provides a powerful technique for detecting microdefects of nanometre size and random distribution. This represents an important extension of X-ray topography to the field of crystal-defect characterization.

This work was supported by the National Natural Science Foundation of China.

References

CLAEYS, C. & VANHELLEMONT, J. (1993). *J. Cryst. Growth*, **126**, 41–49.
DEDERICHS, P. H. (1973). *J. Phys. F*, **3**, 471–475.
GÖSELE, U. & TAN, T. Y. (1982). *Appl. Phys.* A**28**, 79–82.
IIDA, S., SUGIYAMA, H., SUGITA, Y. & KAWATA, H. (1988). *Jpn. J. Appl. Phys.* **27**, 1081–1087.
KATO, N. (1980). *Acta Cryst.* A**36**, 763–769, 770–778.
MAI, Z. H., CUI, S.-F., WANG, C.-Y., WU, L.-S., LI, H.-P., CHEN, G.-X., ZHOU, S.-R. & YE, S.-C. (1990). *Mod. Phys. Lett.* B**4**, 625–634.
PATEL, J. R. (1973). *J. Appl. Phys.* **44**, 3903–3907.
SUGITA, Y., SUGIYAMA, H., IIDA, S. & KAWATA, H. (1987). *Jpn. J. Appl. Phys.* **26**, 1903–1906.

Acta Cryst. (1994). A**50**, 730–736

The Reduction of *N*-Beam Scattering from Noncentrosymmetric Crystals to Two-Beam Form

BY A. F. MOODIE AND H. J. WHITFIELD

Department of Applied Physics, Royal Melbourne Institute of Technology, Box 2476 *W, Melbourne, Victoria* 3001, *Australia*

(*Received* 8 *February* 1994; *accepted* 6 *April* 1994)

Abstract

It is shown that certain noncentrosymmetric seven-beam configurations can be reduced to two-beam form. This is exemplified for the space group of α-quartz, namely $P3_121$, with the incident beam along [001]. Explicit eigenvalues and eigenvectors are given for this case and it is shown that the two-beam form is independent of the imaginary parts of the structure amplitudes. The reduction is shown to result from five zero projectors rather than confluence, although confluence is present. An exhaustive list of the 15 reducible noncentrosymmetric space groups is obtained.